Title. Basolateral amygdala astrocytes are engaged by the acquisition and expression of a contextual fear memory.

Authors. Rebecca L. Suthard*, Ryan A. Senne*, Michelle D. Buzharsky, Rebecca H. Cole, Steve Ramirez.
* = co-first

Abstract.
Astrocytes are key cellular regulators within the brain. The basolateral amygdala (BLA) is implicated in fear memory processing, yet most research has entirely focused on neuronal mechanisms, despite a significant body of work implicating astrocytes in learning and memory. In the present study, we used *in vivo* fiber photometry to record from amygdalar astrocytes across fear learning, recall, and three separate periods of extinction. We found that BLA astrocytes robustly responded to foot-shocks during acquisition, that their activity remained remarkably elevated across days in comparison to unshocked control animals, and that their increased activity persisted throughout extinction. Further, we found that astrocytes responded to the initiation and termination of freezing bouts during contextual recall, and this behavior-locked pattern of activity did not persist throughout the extinction sessions. Our work presents a real-time role for amygdalar astrocytes in fear processing and provides new insight into the emerging role of these cells in cognition and behavior.

Main Points:

- BLA astrocytes robustly respond to foot-shock.
- Shock animals had significantly different calcium events across fear learning compared to no-shock controls.
- Calcium peri-events were present at initiation and termination of freezing during recall.

1) Introduction.

Memory acquisition, recall, and extinction are critical phases for information processing in the brain; disruption of any of these processes can lead to pathological states of cognition and behavior. Fear memories are one of the most well studied forms of memory, and have been shown to recruit numerous brain areas including the hippocampus and basolateral amygdala (BLA). Specifically, during Pavlovian fear conditioning, the CA1 and CA3 subregions of the hippocampus (HPC) relay information to the amygdala via the ventroangular pathway or through the entorhinal cortex (EC), which also projects to the prefrontal cortex (PFC). The amygdala then is thought to send output to the central amygdala (CeM) which in turn sends output to the lateral hypothalamus or periaqueducteal gray (PAG) to alter the sympathetic nervous system and gate freezing behavior, respectively. This complex fear circuitry is necessary for proper memory processing and these regions each differentially contribute to the behavioral expression of fear.

Recent work has demonstrated the active involvement of astrocytes in cognition and behavior by regulating synaptic plasticity, supporting metabolic homeostasis, modulating neurotransmitter action and releasing their own gliotransmitters to exert wide-ranging effects on the brain (Araque et. al., 2014; Bezzi et. al., 2001; Araque et. al., 2001; Araque et. al., 1999; Haydon et. al., 2001; Perea & Araque, 2005; Perea et. al., 2009; Parpura et. al., 1994; Porter et. al., 1997; Volterra et. al., 2005; Koizumi et. al., 2005; Covelo et. al., 2018; Di Castro et. al., 2011; Fellin et. al., 2004; Durkee et. al., 2019). Broadly, chemogenetic and optogenetic perturbations of astrocytic functioning have been shown to impair or enhance both recent and remote memory in the hippocampus, amygdala and prefrontal cortex (Kol et. al. 2020; Adamsky et. al., 2018; Li et. al.. 2020; Martin-Fernandez et. al., 2017; Liao et. al., 2017; Fan et. al., 2021). The effects of these manipulations depend heavily on the brain region of interest, the signaling pathways perturbed and the time point of manipulation during behavior. Mounting evidence suggests that astrocytes may modulate local and projection-specific network activity in memory processes (Kol et. al., 2020; Martin-Fernandez et. al., 2017). For example, a recent study demonstrated that hippocampal dorsal CA1 (dCA1) astrocytic Gq activation during contextual fear conditioning is sufficient to promote long-term potentiation and enhance subsequent recall in mice, whereas neuronal activation does not (Adamsky et. al., 2018). Further research in the BLA has shown that fear conditioning itself downregulates astrocytic Rac1 to facilitate the formation of a conditioned fear memory (Liao et. al., 2017; Fan et. al., 2021). Additionally, BLA astrocytic Gq pathway activation during fear conditioning increased auditory memory, but not contextual memory retrieval, dissociating the role of these cells in multiple types of aversive learning (Lei et. al., 2022). Finally, Gq activation of astrocytes in the BLA after cued fear extinction training decreases freezing levels during extinction recall 24 hours later (Shelkar et. al., 2021). This evidence supports bidirectional astrocyte-neuron communication in multiple subdivisions of the amygdala and suggests their active control over the functional connectivity of the amygdala with other canonical fear-learning 'hubs'.

Despite the recent interest in astrocytic contributions to memory, these studies predominantly use perturbation approaches (e.g. cell-type-specific activation or inhibition of cellular activity), whereas neuronal investigations may now multiplex these causal approaches with optical imaging to gain real-time insight on cellular activity during behavior. Still, there are relatively few studies utilizing these approaches, even with newer genetically-encoded calcium indicators (GECIs) and transgenic mouse lines that are capable of preferentially

targeting astrocytes for dynamic calcium recordings across behavior (Corkrum et. al., 2020; Lin et. al., 2021; Qin et. al., 2020; Lines et. al., 2020; Tsunematsu et. al., 2021). Understanding the activity of astrocytes in real-time is essential for understanding cognition, especially given that the brain predominantly consists of glia.

The BLA is a key hub for valence-specific memories. Prior work has shown that the BLA is necessary for the encoding and retrieval of the emotional component of fearful experiences, and lesioning experiments have shown that its disruption strongly inhibits proper emotional responses (Zhang and Li, 2018; Maren, Ahranov, and Fanselow 1996; Maren 1999). Furthermore, the BLA has also been shown to be necessary for the acquisition and extinction of contextual fear memory in mice, suggesting it plays a key role in every stage of fear learning. Despite the relatively large body of literature implicating the BLA in fear conditioning, almost all of this work has focused on neuronal responses, and there is currently a limited understanding on how astrocytic calcium responses in the BLA manifest across fear acquisition, recall, and contextual extinction.

To address this, we use freely-moving fiber photometry (Gunaydin et. al., 2014; Cui et. al., 2014) to record population-level astrocytic calcium dynamics across the classic contextual fear conditioning (CFC) paradigm. First, we find that astrocytes in the BLA are shock-responsive, which suggests that astrocytes in this amygdalar sub-region process salient and/or aversive-related stimuli. Next, we find that astrocytes in the shock condition displayed unique calcium events across fear learning compared to the unshocked control group. Finally, we observed calcium peri-events at the initiation and termination of freezing bouts during recall, but this did not persist into extinction sessions. Together, our experiments provide a more comprehensive understanding of the contributions of glial cells to learning and memory processes. Perturbation of these cells during extinction memory formation and maintenance may pave the way for more successful therapeutic interventions in humans with disorders of maladaptive fear learning, such as Post-Traumatic Stress Disorder (PTSD).

2) Methods

2.1) Animals

Wild type, male C57BL/6J mice (P29-35; weight 17-19g; Charles River Laboratories) were housed in groups of 4-5 mice per cage. The animal facilities (vivarium and behavioral testing rooms) were maintained on a 12:12 hour light cycle (0700-1900). Mice received food and water *ad libitum* before and after surgery. Following surgery, mice were group-housed with littermates and allowed to recover for 3 weeks before experimentation. All subjects were treated in accord with protocol 201800579 approved by the Institutional Animal Care and Use Committee (IACUC) at Boston University.

2.2) Stereotaxic Surgery

For all surgeries, mice were initially anesthetized with 3.0-3.5% isoflurane inhalation during induction and maintained at 1-2% isoflurane inhalation through stereotaxic nosecone delivery (oxygen 1L/min). Ophthalmic ointment was applied to the eyes to provide adequate lubrication and prevent corneal desiccation. The hair on the scalp above the surgical site was removed using Veet hair removal cream and subsequently cleaned with alternating applications of betadine solution and 70% ethanol. 2.0% lidocaine hydrochloride (HCl) was injected subcutaneously as local analgesia prior to midsagittal incision of the scalp skin to expose the skull. 0.1mg/kg

(5mg/kg) subcutaneous (SQ) dose of meloxicam was administered at the beginning of surgery. For fiber photometry implant surgeries, all animals received a unilateral craniotomy with a 0.5-0.6 mm drill-bit for basolateral amygdala (BLA) injections.

A 10μL airtight Hamilton syringe with an attached 33-gauge beveled needle was slowly lowered to the coordinates of BLA: -1.40 anteroposterior (AP), -3.20 mediolateral (ML) and -4.80 dorsoventral (DV). All coordinates are given relative to bregma (mm). A volume of 500nL of AAV-GfaABC1D-cyto-GCaMP6f-SV40 (Penn Vector Core) was injected at 50nL/min using a microinfusion pump for the BLA coordinate (UMP3; World Precision Instruments). After the injection was complete, the needle remained at the target site for 7-10 minutes post-injection before removal. Following viral injection, a unilateral optic fiber (200μm core diameter; 1.25mm ferrule diameter) was implanted at the site of injection. The implant was secured to the skull with a layer of adhesive cement (C&M Metabond) followed by multiple layers of dental cement (Stoelting). Following surgery, mice were injected with 0.1mg/kg intraperitoneal (IP) dose of buprenorphine (volume administered was dependent on the weight of the animal at the time of surgery). They were placed in a recovery cage with a heating pad until fully recovered from anesthesia. To allow for recovery and viral expression, we waited 3-4 weeks before beginning our behavioral paradigm. Histological assessment verified unilateral viral targeting and data from off-target injections were not included in analyses.

2.3) Fiber Photometry

A 470-nm LED (Neurophotometrics; FP3002) delivered an excitation wavelength of light to astrocytes expressing GCaMP6f via a single fiber optic implant. The emitted 530-nm signal from the indicator was collected via this same fiber, spectrally-separated using a dichroic mirror, passed through a series of filters and was focused on a scientific camera. Calcium-independent isosbestic signals were simultaneously captured by alternating excitation with 415-nm LED to dissociate motion, tissue autofluorescence, and photobleaching from true changes in fluorescence. All wavelengths were interleaved and collected simultaneously using Bonsai (Lopes et. al., 2015). The sampling rate for the signals was 28Hz (28 frames per second). Time series were analyzed using an in-house pipeline and fluorescence signals were normalized to the median and transformed to a z-score to allow for comparison of event amplitude (peak height; % dF/F), frequency (Hz), total fluorescence (area under the curve) and duration (full-width half maximum; seconds). Statistical analyses were performed using Python and data reported as Mean ± SEM.

2.4) Behavioral Testing

On Day 1, mice were placed into the shock context (Cxt A) where they underwent a 360s contextual fear conditioning session. Footshocks (1.5mA, 2s duration) were administered at the 120, 180, 240 and 300 second time points at 1.5mA intensity. On Day 2, mice were placed back in Cxt A for 360s of recall where they received shock on the previous day. There were no shocks administered during this session. On Days 3- 5, mice were placed back in Cxt A for 900s without shock administration to extinguish the fear memory across days. At the completion of extinction testing, mice in the no-shock group were administered a single 1.5mA footshock to confirm the presence of calcium signal. All of these sessions took place in mouse conditioning chambers

(Coulbourn Instruments) with metal-panel side walls, plexiglass front and rear walls and a stainless-steel grid floor composed of 16 grid bars. The grid floor was connected to a precision animal shocker to deliver 2 second duration, 1.5mA foot shocks. A video camera was mounted on a tripod in a front-facing orientation to the conditioning chamber. The chambers were cleaned with 70% ethanol solution prior to each animal placement. All behavioral testing was performed during the animal's light-cycle.

2.6) Immunohistochemistry and Image Analysis

On Day 6, mice were overdosed with 3% isoflurane and perfused transcardially with cold (4°C) phosphate-buffered saline (PBS) followed by 4% paraformaldehyde (PFA; pH = 7.4) in PBS. Brains were extracted and kept in PFA at 4°C for 24-48 hours and transferred to a 30% sucrose in PBS solution. Brains were sectioned into 50μm thick coronal sections with a vibratome and collected in cold PBS or 0.01% sodium azide in PBS for long-term storage. Sections were washed three times for 10-15 minutes with PBS or PBST to remove 0.01% sodium azide used for storage. Vibratome sections were incubated for 2 hours in PBS combined with 0.2% Triton (PBST) and 5% bovine serum albumin (BSA) on a shaker at room temperature. Sections were incubated in the primary antibodies (1:1000 mouse monoclonal anti-GFAP [NeuroMab]; 1:1000 rabbit polyclonal anti-Iba1 [Wako]; 1:500 guinea pig anti-NeuN [SySy]) diluted in PBST/1% BSA at 4°C for 24 or 48 hours. The slices were washed three times for 10-15 minutes each in 1xPBS. The secondary antibodies were diluted in secondary antibody solution (PBST/1% BSA) and incubated for 2 hours at room temperature. The following secondary antibodies were used: 1:1000 Alexa 555 anti-mouse [Invitrogen], 1:1000 Alexa 555 anti-rabbit [Invitrogen], 1:200 Alexa 555 anti-guinea pig [Invitrogen]. The sections were then washed three times with 1xPBS or PBST for 10-15 minutes each and mounted using Vectashield Mounting Medium with DAPI (Vector Laboratories). Once dry, slides were sealed with clear nail polish on each edge and stored in a slide box in the fridge (4°C). Mounted slices were imaged using a confocal microscope (Zeiss LSM800, Germany). Brains from all mice used in fiber photometry experiments were analyzed to check adequate fiber location and proper and selective viral expression. Animals that did not meet the criteria for proper fiber location and virus expression were discarded.

The cellular specificity of the GCaMP6f viral vectors was tested by immunohistochemical analysis of randomly selected areas of the vCA1. Of the 2256 cells expressing GCaMP6f (n = 3 mice; 3 slices), 2242 were astrocytes (identified by GFAP), resulting in a specificity of 99.4%. Of the 662 cells expressing GCaMP6f (n=3 mice; 3 slices), 4 were microglia (identified by Iba-1), resulting in a specificity of 0.6%. Of the 1064 cells expressing GCaMP6f (n = 3 mice; 3 slices), 0 were neurons (identified by NeuN), resulting in a specificity of 0%. Finally, of 2381 GFAP+ astrocytes, 2251 were GCaMP6f+ (n=3 mice; 3 slices), resulting in a penetrance of 98.49%.

2.6) Behavioral Analysis

AnyMaze was used for supervised automated analysis of freezing bout initiation and termination. This behavioral data was time locked to our fiber photometry time series data for analysis.

2.7) Statistical and Fiber Photometry Analysis

All statistical analysis and subsequent photometry analysis was performed via custom python scripts freely available at https://github.com/rsenne/RamiPho. Our environment was built off of scipy (ver. 1.7.3),

statsmodels (ver. 0.13.2), numpy (ver. 1.22.3), pandas (ver. 1.4.2), matplotlib (ver. 3.5.1), numba (ver. 0.55.2), and seaborn (ver. 0.11.2).

All photometry signals were baseline corrected using an adaptive iteratively reweighted penalized least squares method (Zhang, Chen, and Liang, 2010). We then performed a simple kernel smoothing to increase the signal to noise ratio. For "event detection" we used a method published in prior literature (Howe et al. 2019). DF/F was calculated by subtracting the median of the trace from the current fluorescence value and then dividing by the median, giving a percent difference from the median or "baseline". We then found any peaks greater than 1 standard deviation away from the mean, in both the positive and negative direction. We then determined the minimum width such that the ratio of positive to total transients (negative and positive) was greater than or equal to 0.99. Any transients below this width were subsequently discarded.

For peri-event analysis, we used a tCI method as proposed previously (Jean-Richard-dit-Bressel, Clifford & McNalley, 2020). For each window of interest, we calculated a 95%, 99% and 99.9% confidence interval. If the CI did not contain the null assumption (dF/F = median of the event window), for a period greater than 0.5 s we concluded that a significant peri-event occurred.

3) Results.

Astrocytes in the basolateral amygdala are actively involved in fear memory (Liao et. al., 2017; Fan et. al., 2021; Lei et. al., 2022; Shelkar et. al., 2021; Stehberg et. al., 2012), but their real-time dynamics during the acquisition and maintenance of conditioned fear in mice is relatively unknown. We monitored astrocyte calcium levels in the BLA using fiber-photometry in freely behaving mice across the acquisition, retrieval, and extinction of conditioned fear. Wild type mice were injected unilaterally with AAV-GfaABC1D-cyto-GCaMP6f to express the genetically-encoded calcium indicator (GECI) GCaMP6f selectively in astrocytes (Figure 1A-C). To quantify the penetrance and specificity of our viral system, we co-labeled GCaMP6f+ cells with GFAP, Iba-1 and NeuN, markers for astrocytes, microglia and neurons, respectively (Figure 1D-F). Of 2381 GFAP+ cells, 2251 were GCaMP6f+ (n=3; 4 slices/mouse), resulting in a penetrance of 98.49% (Figure 1D, F). Of 662 GCaMP6f+ cells, 4 were Iba1+, resulting in a specificity of 0.604% for microglia (Figure 1E-F). Of 1064 GCaMP+ cells, 0 were NeuN+, resulting in a specificity of 0.0% for neurons (Figure 1E-F). Finally, of 2256 GCaMP+ cells, 2242 were GFAP+, resulting in a specificity of 99.4% for astrocytes (Figure 1E-F).

To test the hypothesis that astrocytes play an active role in the acquisition and maintenance of contextual fear, we used *in vivo* fiber photometry to record their activity across all experimental days of our behavioral task (Figure 1F-G). Recent literature using calcium imaging in ventral hippocampus (vHPC) has shown that a subset of BLA-vHPC projecting neurons were responsive to aversive shock during CFC (Jimenez et. al., 2020). This provides ample evidence that BLA neurons and astrocytes are also likely to be shock-responsive. On Day 1, mice underwent contextual fear conditioning with the administration of 1.5mA foot shocks at 120, 180, 240 and 300 second timepoints (Figure 1G). To assess whether BLA astrocytes responded specifically to footshock, we performed peri-event analysis to determine if calcium transients were temporally locked to footshock. We used a tCI confidence interval method to classify significant perievents around a time-

point of interest as previously described (Jean-Richard-dit-Bressel, Clifford & McNalley, 2020; *See Methods*). Astrocytes in the shock group displayed robust increases in population-level calcium at the onset of each foot shock during the session compared to the no-shock condition, as shown by a representative calcium time series (% dF/F) from each group (Figure 2A) and raster plots (z-scored % dF/F) including all mice from each group (Figure 2C, E). Further analysis revealed that the shock group had significantly increased % dF/F from baseline after the onset of each foot shock compared to the no-shock condition (Footshock peri-event analysis; 99% confidence interval (CI))(Figure 2B). Specifically, the shock group had an increase of 44.6% dF/F from baseline after the onset of each footshock, on average, compared to 1.6% increase dF/F for the no-shock condition (Independent samples t-test; Welch's correction, $p=0.0022$) (Figure 2C). For CFC, we calculated event metrics such as peak height, full-width half max (FWHM), area under the curve (AUC), and frequency (events/minute) for shock and no-shock groups. The shock group had significantly increased event peak height, increased AUC, and decreased full-width half max (FWHM) compared to no shock during CFC ([Peak height: Independent t-test; Welch's correction, $p=0.0019$][AUC: Independent t-test; Welch's correction, $p=0.0011$][FWHM: Independent t-test; $p<0.0001$][Frequency: Independent t-test; $p=0.069$ (ns)](Figure 2F-H). Behaviorally, mice in the shock group had a higher freezing across the 360s session, compared to the no-shock group that did not experience a foot shock (Independent t-test; $p<0.0001$)(Figure 2J). The shock group successfully acquired fear across the CFC session compared to the no-shock condition (Two-way ANOVA with repeated measures (RM); Interaction: $F(5, 80) = 10.14$, $p<0.0001$; Time bin: $F(1.750, 28.00) = 13.02$, $p=0.0002$; Group: $F(1, 16) = 23.59$, $p=0.0002$; Subject: $F(16, 80) = 4.593$, $p<0.0001$)(Figure 2K). *Post-hoc* analysis demonstrated significant group differences in freezing at the 180, 240, 300 and 360 second time bins (Sidak's multiple comparisons: 180s: $p=0.0167$; 240s: $p=0.0015$; 300s: $p<0.0001$; 360s: $p<0.0001$)(Figure 2K). Together, the calcium events for the shock condition (i.e. higher amplitude, higher total fluorescence, shorter duration events) suggest that astrocytes become more active after the presentation of a salient stimulus, as suggested by previous literature demonstrating that these cells in dCA1 are responding in a stimulus-dependent manner (Adamsky et. al., 2018).

Recent studies have shown that manipulation of astrocytes during retrieval of a conditioned fear memory does not affect recent or remote memory recall, though their activity within a given session remained unmeasured (Adamsky et. al., 2018; Kol et. al., 2020). To that end, we investigated the real-time dynamics of these cells in mice that received foot shock vs. neutral exposure to the same context. On Day 2 of our experiment, mice underwent contextual recall without the presence of the unconditioned stimulus (US; foot shock)(Figure 1F-G). When comparing population-level calcium activity across the shock and no-shock groups, we observed stark differences in the engagement of astrocytes (Figure 3A-B, D). Specifically, we observed that the presence of the US (i.e. footshock) during fear conditioning continued to engage astrocytes when placed back in the original context, while the no-shock group displayed low levels of calcium activity. As the US is the most salient manipulated variable between these two groups, we speculate that astrocytes may be engaged in a learning-dependent manner within the basolateral amygdala (BLA). We also tested the hypothesis that astrocytes modulate their behavior in response to the onset and/or offset of freezing. There were significant peri-events, where the event started prior to the initiation of freezing (Freeze onset peri-event analysis; 95% CI)(Figure 3C) and immediately after the onset of freezing (Freeze offset peri-event analysis; 95% CI)(Figure

3E). Behaviorally, mice in the shock group exhibited increased freezing compared to the no-shock condition that did not receive the CS-US pairing (Mann-Whitney U-test; $p<0.0001$)(Figure 3F). Across the recall session, mice in the shock group maintained higher levels of freezing compared to no-shock controls (Two-way ANOVA RM; Interaction: $F(5, 80) = 1.163$, $p=0.3346$; Time Bin: $F(5, 80) = 1.906$, $p=0.1024$; Group: $F(1, 16) = 93.18$, $p<0.0001$; Subject: $F(16, 80) = 8.924$, $p<0.0001$) (Figure 3G). *Post-hoc* analysis across groups supported significantly higher levels of freezing in the shock condition during recall across all time bins (Sidak's multiple comparisons: 60s: $p<0.0001$; 120s: $p<0.0001$; 180s: $p<0.0001$; 240s: $p<0.0001$; 300s: $p<0.0001$; 360s: $p<0.0001$) (Figure 3G). Furthermore, to quantify these differences in the traces across groups, we calculated the same average event metrics mentioned above (i.e. peak height, FWHM, AUC, frequency). The shock group had increased average peak height, decreased FWHM, increased AUC, and there were no differences in frequency of events across the session ([Peak height: Independent t-test; Welch's correction, $p=0.0009$][AUC: Independent t-test; Welch's correction, $p=0.0156$][FWHM: Independent t-test; Welch's correction, $p=0.0005$][Frequency: Independent t-test; Welch's correction, $p=0.3642$).(Figure 3H-K). This suggests that after context-shock association, astrocytes retain similar calcium dynamics on the following day when placed back in the conditioned environment in the absence of shock.

To further evaluate the experience-dependent role of astrocytic calcium across the extinction of contextual fear, mice underwent three days of extinction on Days 3-5 of our behavioral paradigm (Figure 1F-G). When comparing astrocytic calcium levels during extinction, we observed higher population activity in the shock group in the absence of the original US compared to the no-shock condition across all three days (Figure 4A-I). This suggests that astrocytes are continuing to be engaged in the shock group, and perhaps in a memory-dependent manner as an extinction memory is being formed across days. The no shock group displayed minimal calcium activity, which may be due to continued exploration of a novel environment as it becomes familiar (Qin et. al., 2020). Furthermore, to quantify these differences across groups, we calculated event metrics for each extinction session. For extinction day 1, the shock condition had calcium events with increased amplitude, increased AUC, decreased FWHM (i.e. duration of event), and decreased frequency ([Peak height: Independent t-test; Welch's correction, $p=0.0016$][AUC: Independent t-test; Welch's correction, $p=0.0036$][FWHM: Mann-Whitney U-test, $p=0.0019$][Frequency: Independent t-test, $p=0.0253$])(Figure 4J-M). For extinction day 2, the shock condition had calcium events with increased amplitude, increased AUC, decreased FWHM and no difference in frequency ([Peak height: Independent t-test, $p=0.0001$][AUC: Independent t-test, $p<0.0001$][FWHM: Mann-Whitney U-test, $p=0.0043$][Frequency: Independent t-test, $p=0.2050$])(Figure 4J-M). Finally, for extinction day 3, the shock condition had calcium events with increased amplitude, but no significant differences in FWHM, AUC or frequency compared to no-shock controls ([Peak height: Independent t-test, $p=0.0010$][AUC: Independent t-test; Welch's correction, $p=0.126$][FWHM: Independent t-test, $p=0.1447$][Frequency: Independent t-test, $p=0.3851$)(Figure 4J-M). Interestingly, this suggests that astrocytes are initially impacted by the presence of the foot shock during CFC, but do not adapt further across extinction days. To further investigate astrocytic calcium responses to freezing behaviors, peri-event metrics for the onset and offset of freezing were calculated as previously performed in contextual recall. Interestingly, astrocytic calcium in the shock group was not responsive to the onset or offset of freezing behavior for all extinction sessions (Freeze onset & offset peri-event analysis; ns)(Figure 5A-B, D-E, G-H).

Behaviorally, mice in the shock group exhibited higher average levels of freezing than the no-shock condition group for all three days ([Extinction 1: Independent t-test; Welch's correction, p<0.0001][Extinction 2: Independent t-test; Welch's correction, p=0.0042][Extinction 3: Independent t-test; Welch's correction, p=0.0123])(Figure 5J). For each extinction session, shocked mice displayed higher levels of freezing at each time bin than no-shock controls ([Extinction 1: Two-way ANOVA RM; Interaction: F (14, 210) = 1.140, p=0.3247; Time bin: F (4.530, 67.95) = 1.726, p=0.1467; Group: F (1, 15) = 22.92, p=0.0002; Subject: F(15, 210) = 18.83, p<0.0001)][Extinction 2: Two-way ANOVA RM; Interaction: F (14, 168) = 1.204, p=0.2765; Time Bin: F (4.306, 51.68) = 1.364, p=0.2574; Group: F (1, 12) = 18.86, p=0.0010; Subject: F (12, 168) = 30.92, p<0.0001][Extinction 3: Interaction: F (14, 168) = 0.9191, p=0.5395; Time bin: F (3.186, 38.23) = 1.160, p=0.3392; Group: F (1, 12) = 12.14, p=0.0045; Subject: F (12, 168) = 25.16, p<0.0001])(Figure 5C, F, I). Specifically, *post-hoc* analysis for extinction days revealed specific time bin differences across groups, and this declines across extinction days([Extinction 1: Sidak's multiple comparisons; 120s: p=0.0470; 180s: p=0.0202; 240s: p=0.0016; 300s: p=0.0013; 360s: 0.0002; 420s: p=0.0003; 480s: p=0.0007; 540s: p=0.0020; 600s: p=0.0028; 660s: p=0.0094; 720s: p=0.0073; 780s: p=0.0155; 900s: p=0.0105][Extinction 2: Sidak's multiple comparisons; 240s: p=0.0039; 300s: p=0.0187; 420s: p=0.0181][Extinction 3: Sidak's multiple comparisons; 360s: p=0.0094])(Figure 5C, F, I). Overall, our data suggest that astrocytic calcium remains elevated even as freezing levels decline naturally across extinction sessions.

4) Discussion.

Our results demonstrate that BLA astrocytes are differentially involved in the acquisition, recall, and extinction of a contextual fear memory. Strikingly, these astrocyte populations in the no-shock groups showed low levels of calcium dependent activity relative to the shocked group. These results corroborate previous research demonstrating that astrocytic populations are active specifically during salient experiences (Adamsky et. al., 2018). Furthermore, this could be related to an increased demand for neuronal metabolic support due to cellular activity recruited during memory formation. Recent models suggest that astrocytes become active during metabolically taxing experiences to support memory encoding and consolidation by providing astrocytically derived lactate to neuronal populations to increase ATP production (Steinman et. al., 2016; Adamsky & Goshen, 2018; Alberini et al. 2018). In line with this possibility, in our study mice that did not associate a noxious stimulus to the context displayed less activity than the shocked group. This could indicate that during memory acquisition, where a CS is paired with a US, astrocytic populations become involved to maintain this memory association. As the BLA preferentially parses salient information (Sengupta et. al., 2018; Pryce et. al., 2018), this could explain the lack of strong calcium events in the no-shock group, whereas in a structure that processes both associations and emotional salience (Zheng et. al., 2017; Eichenbaum, Schoenbaum, Young & Bunsey, 1996), such as the hippocampus, we predict to see reliable but increased events during contextual exploration and after CS-US pairing. Relatedly, and given that astrocyte assemblies are remarkably disengaged before the onset of foot shock during CFC in our study, future experiments may test whether populations of astrocytes are necessary for proper fear expression, and if after such salient experiences, BLA neurons require glial participation for stable memory correlates.

Interestingly, we only observed differences in the event geometry in the shock group when animals are undergoing CFC. This could indicate there are two distinct populations of cells, one which becomes active for memory encoding and maintenance, whereas the other is there to process incoming sensory input into the BLA only during the experience and becomes subsequently inactive. Furthermore, while the no-shock animals display minimal calcium transients these transients are significantly wider, possibly in response to exploring the novel context. This could be explained by the observation that AUC for these transients was also significantly lower for these animals, suggesting their was less overall calcium binding and subsequent recorded fluorescence, and thus indicating their may be cells that had sustained activity in response to a non-discrete stimuli, in contrast to something well defined like foot-shock. Furthermore, peri-events were observed in the recall session, before the initiation of freezing, and after the termination. It could be possible that astrocytes ramp up their activity to either help induce a state of freezing or come online in response to increased neuronal activation immediately prior to bouts of freezing. Regarding the offset of a freezing bout specifically, it could be possible that astrocytes play a functional role in suppressing fear states within the BLA, though it is important to note that separate studies have also implicated their role in modulating locomotion (Qin et. al., 2020)--thus, as termination of freezing by definition requires movement, these two explanations remain to be reconciled without further experiments. Notably, we did not notice these elevations in calcium activity at the onset or offset of freezing during extinction. This could be due to the difference in session length causing changes to how these cells respond after the initial six-minutes, or it could be that after this initial exposure some subsequent learning has occurred causing these cells to respond to different local cues or internal states.Whilefiber photometry renders this possibility difficulty to test due to the lack of cell-specific granularity it affords, these hypotheses would be interesting to explore with higher resolution *in vivo* one-photon imaging approaches as it would allow us to visualize multiple subpopulations of BLA astrocytes, which could explain the diverse milieu of these signals.

While our results demonstrate a functional role of astrocytes in fear learning, the BLA is known to process additional salient information including fear, reward, novelty, etc. For instance, recent studies have shown that there are heterogeneous, genetically defined, populations within the BLA which may preferentially respond to a variety of stimuli and valences (Kim et. al., 2016). While our experiments did not tease out any valence-specific contributions of astrocytic calcium activity, future studies may deliver multiple valence-specific stimuli (e.g. sweetened condensed milk, social interaction, restraint stress) to animals while recording the corresponding calcium transients in the BLA. We posit that the BLA will display robust calcium dynamics to both positive and negative stimuli, albeit in partially separate populations of cells. This is consistent with recent literature showing that there are genetically-defined populations of cells along the anterior-posterior axis of the BLA that process fear and reward uniquely (Kim et. al., 2016).

While this work provides a role for astrocytes in conditioned fear, an ongoing issue surrounds whether astrocytes are mere support cells for neurons or if they actively encode information necessary for cognitive processes. Future experiments may concurrently record from neuronal populations to identify putative relationships between each cell type, and how real-time interplay between these populations supports learning and memory processes. A tantalizing possibility that combines neuron-glia relationships with neuromodulatory influences is that BLA astrocytes are necessary for proper adrenergic signaling which has been proposed in prior

work (Gao et. al., 2016; Akther & Hirase, 2021). Also, it has been shown that CFC induces a downregulation of astrocytic Rac-1 (Liao et. al., 2017; Fan et. al., 2021), promoting astrocytic plasticity, which may explain our observed differences in calcium events between our two groups in that this increased astrocytic plasticity could be necessary for remodeling synaptic connections for continued signaling.

Finally, future studies may causally dissect the role of astrocytes by Gq or Gi pathway activation in these populations during recall or extinction to determine if cellular manipulation is capable of inducing either a memory enhancing or amnesic response to fear learning. As astrocytes do not have typical "inhibition/excitation" properties which are more typically associated with neurons (Durkee et. al., 2019; Van Den Herrewegan et. al., 2021), future research may take its amore complex signaling pathways into account and yield crucial information in how astrocytes participate at the tripartite synapse to facilitate the learning of conditioned fear. Indeed, higher resolution single-cell and populating imaging methods, combined with causal perturbation strategies, could be used to further delineate the role of these cells in memory formation and expression. Overall, our results suggest an active role of astrocytes in contextual fear learning within the BLA and reveal their dissociable role in contributing to memory recall and extinction.

5) Data Availability Statement.

The data that support the findings of this study are available from the corresponding author upon reasonable request.

6) Acknowledgements.

This work was supported by a Ludwig Family Foundation grant, an NIH Early Independence Award (DP5 OD023106-01), an NIH Transformative R01 Award, a Young Investigator Grant from the Brain and Behavior Research Foundation, the McKnight Foundation Memory and Cognitive Disorders award, the Pew Scholars Program in the Biomedical Sciences, the Air Force Office of Scientific Research (FA9550-21-1-0310), the Center for Systems Neuroscience and Neurophotonics Center at Boston University. The authors would also like to thank Fraser and Jeffrey Weiss for helpful comments and useful suggestions on the manuscript.

7) References.

1. Adamsky, A., & Goshen, I. (2018). Astrocytes in Memory Function: Pioneering Findings and Future Directions. *Neuroscience*, *370*, 14–26. https://doi.org/10.1016/J.NEUROSCIENCE.2017.05.033
2. Adamsky, A., Kol, A., Kreisel, T., Doron, A., Ozeri-Engelhard, N., Melcer, T., Refaeli, R., Horn, H., Regev, L., Groysman, M., London, M., & Goshen, I. (2018). Astrocytic Activation Generates De Novo Neuronal Potentiation and Memory Enhancement. *Cell*, *174*(1), 59-71.e14. https://doi.org/10.1016/j.cell.2018.05.002
3. Akther, S., & Hirase, H. (2022). Assessment of astrocytes as a mediator of memory and learning in rodents. *Glia*, *70*(8), 1484–1505. https://doi.org/10.1002/GLIA.24099
4. Alberini, C. M., Cruz, E., Descalzi, G., Bessières, B., & Gao, V. (2018). Astrocyte glycogen and lactate: new insights into learning and memory mechanisms. *Glia*, *66*(6), 1244. https://doi.org/10.1002/GLIA.23250
5. Araque, A., Carmignoto, G., & Haydon, P. G. (2001). Dynamic signaling between astrocytes and neurons. *Annual Review of Physiology*, *63*, 795–813. https://doi.org/10.1146/ANNUREV.PHYSIOL.63.1.795
6. Araque, A., Carmignoto, G., Haydon, P. G., Oliet, S. H. R., Robitaille, R., & Volterra, A. (2014). Gliotransmitters travel in time and space. *Neuron*, *81*(4), 728–739. https://doi.org/10.1016/J.NEURON.2014.02.007
7. Araque, A., Parpura, V., Sanzgiri, R. P., & Haydon, P. G. (1999). Tripartite synapses: Glia, the unacknowledged partner. *Trends in Neurosciences*, *22*(5), 208–215. https://doi.org/10.1016/S0166-2236(98)01349-6
8. Bezzi, P., & Volterra, A. (2001). A neuron-glia signaling network in the active brain. *Current Opinion in Neurobiology*, *11*(3), 387–394. https://doi.org/10.1016/S0959-4388(00)00223-3
9. Corkrum, M., Covelo, A., Lines, J., Bellocchio, L., Pisansky, M., Loke, K., Quintana, R., Rothwell, P. E., Lujan, R., Marsicano, G., Martin, E. D., Thomas, M. J., Kofuji, P., & Araque, A. (2020). Dopamine-Evoked Synaptic Regulation in the Nucleus Accumbens Requires Astrocyte Activity. *Neuron*, *105*(6), 1036. https://doi.org/10.1016/J.NEURON.2019.12.026
10. Covelo, A., & Araque, A. (2018). Neuronal activity determines distinct gliotransmitter release from a single astrocyte. *ELife*, *7*. https://doi.org/10.7554/ELIFE.32237
11. Cui, G., Jun, S. B., Jin, X., Luo, G., Pham, M. D., Lovinger, D. M., Vogel, S. S., & Costa, R. M. (2014). Deep brain optical measurements of cell type–specific neural activity in behaving mice. *Nature Protocols*, *9*(6), 1213. https://doi.org/10.1038/NPROT.2014.080
12. di Castro, M. A., Chuquet, J., Liaudet, N., Bhaukaurally, K., Santello, M., Bouvier, D., Tiret, P., & Volterra, A. (2011). Local Ca2+ detection and modulation of synaptic release by astrocytes. *Nature Neuroscience*, *14*(10), 1276–1284. https://doi.org/10.1038/NN.2929
13. Durkee, C. A., Covelo, A., Lines, J., Kofuji, P., Aguilar, J., & Araque, A. (2019). Gi/o protein-coupled receptors inhibit neurons but activate astrocytes and stimulate gliotransmission. *Glia*, *67*(6), 1076–1093. https://doi.org/10.1002/GLIA.23589

14. Eichenbaum, H., Schoenbaum, G., Young, B., & Bunsey, M. (1996). Functional organization of the hippocampal memory system. *Proceedings of the National Academy of Sciences of the United States of America*, *93*(24), 13500–13507. https://doi.org/10.1073/PNAS.93.24.13500
15. Fan, X. C., Ma, C. N., Song, J. C., Liao, Z. H., Huang, N., Liu, X., & Ma, L. (2021). Rac1 Signaling in Amygdala Astrocytes Regulates Fear Memory Acquisition and Retrieval. *Neuroscience Bulletin*, *37*(7), 947. https://doi.org/10.1007/S12264-021-00677-W
16. Fellin, T., Pascual, O., Gobbo, S., Pozzan, T., Haydon, P. G., & Carmignoto, G. (2004). Neuronal synchrony mediated by astrocytic glutamate through activation of extrasynaptic NMDA receptors. *Neuron*, *43*(5), 729–743. https://doi.org/10.1016/j.neuron.2004.08.011
17. Gao, V., Suzuki, A., Magistretti, P. J., Lengacher, S., Pollonini, G., Steinman, M. Q., & Alberini, C. M. (2016). Astrocytic β2- Adrenergic receptors mediate hippocampal long- Term memory consolidation. *Proceedings of the National Academy of Sciences of the United States of America*, *113*(30), 8526–8531. https://doi.org/10.1073/PNAS.1605063113/SUPPL_FILE/PNAS.201605063SI.PDF
18. Gunaydin, L. A., Grosenick, L., Finkelstein, J. C., Kauvar, I. v., Fenno, L. E., Adhikari, A., Lammel, S., Mirzabekov, J. J., Airan, R. D., Zalocusky, K. A., Tye, K. M., Anikeeva, P., Malenka, R. C., & Deisseroth, K. (2014). Natural neural projection dynamics underlying social behavior. *Cell*, *157*(7), 1535. https://doi.org/10.1016/J.CELL.2014.05.017
19. Haydon, P. G. (2001). Glia: listening and talking to the synapse. *Nature Reviews Neuroscience 2001 2:3*, *2*(3), 185–193. https://doi.org/10.1038/35058528
20. Howe, M., Ridouh, I., Mascaro, A. L. A., Larios, A., Azcorra, M., & Dombeck, D. A. (2019). Coordination of rapid cholinergic and dopaminergic signaling in striatum during spontaneous movement. *ELife*, *8*. https://doi.org/10.7554/ELIFE.44903
21. Jean-Richard-dit-Bressel, P., Clifford, C. W. G., & McNally, G. P. (2020). Analyzing Event-Related Transients: Confidence Intervals, Permutation Tests, and Consecutive Thresholds. *Frontiers in Molecular Neuroscience*, *13*, 14. https://doi.org/10.3389/FNMOL.2020.00014/XML/NLM
22. Jimenez, J. C., Berry, J. E., Lim, S. C., Ong, S. K., Kheirbek, M. A., & Hen, R. (2020). Contextual fear memory retrieval by correlated ensembles of ventral CA1 neurons. *Nature Communications*, *11*(1). https://doi.org/10.1038/S41467-020-17270-W
23. Kim, J., Pignatelli, M., Xu, S., Itohara, S., & Tonegawa, S. (2016). Antagonistic negative and positive neurons of the basolateral amygdala. *Nature Neuroscience*, *19*(12), 1636. https://doi.org/10.1038/NN.4414
24. Koizumi, S., Fujishita, K., & Inoue, K. (n.d.). *Regulation of cell-to-cell communication mediated by astrocytic ATP in the CNS*. https://doi.org/10.1007/s11302-005-6321-y
25. Kol, A., Adamsky, A., Groysman, M., Kreisel, T., London, M., & Goshen, I. (2020). Astrocytes Contribute to Remote Memory Formation by Modulating Hippocampal-Cortical Communication During Learning. *Nature Neuroscience*, *23*(10), 1229. https://doi.org/10.1038/S41593-020-0679-6
26. Lei, Z., Xie, L., Li, C. H., Lam, Y. Y., Ramkrishnan, A. S., Fu, Z., Zeng, X., Liu, S., Iqbal, Z., & Li, Y. (2022). Chemogenetic Activation of Astrocytes in the Basolateral Amygdala Contributes to Fear Memory Formation by Modulating the Amygdala & Prefrontal Cortex Communication.

International Journal of Molecular Sciences 2022, Vol. 23, Page 6092, *23*(11), 6092. https://doi.org/10.3390/IJMS23116092

27. Li, Y., Li, L., Wu, J., Zhu, Z., Feng, X., Qin, L., Zhu, Y., Sun, L., Liu, Y., Qiu, Z., Duan, S., & Yu, Y. Q. (2020). Activation of astrocytes in the hippocampus decreases fear memory through adenosine A1 receptors. *ELife*, *9*, 1–25. https://doi.org/10.7554/ELIFE.57155
28. Liao, Z., Tao, Y., Guo, X., Cheng, D., Wang, F., Liu, X., & Ma, L. (2017). Fear conditioning downregulates rac1 activity in the basolateral amygdala astrocytes to facilitate the formation of fear memory. *Frontiers in Molecular Neuroscience*, *10*, 396. https://doi.org/10.3389/FNMOL.2017.00396/BIBTEX
29. Lin, Z., You, F., Li, T., Feng, Y., Zhao, X., Yang, J., Yao, Z., Gao, Y., & Chen, J. F. (2022). Entrainment of Astrocytic and Neuronal Ca2+ Population Dynamics During Information Processing of Working Memory in Mice. *Neuroscience Bulletin*, *38*(5), 474–488. https://doi.org/10.1007/S12264-021-00782-W/FIGURES/6
30. Lines, J., Martin, E. D., Kofuji, P., Aguilar, J., & Araque, A. (2020). Astrocytes modulate sensory-evoked neuronal network activity. *Nature Communications 2020 11:1*, *11*(1), 1–12. https://doi.org/10.1038/s41467-020-17536-3
31. Maren, S. (1999). Neurotoxic Basolateral Amygdala Lesions Impair Learning and Memory But Not the Performance of Conditional Fear in Rats. *Journal of Neuroscience*, *19*(19), 8696–8703. https://doi.org/10.1523/JNEUROSCI.19-19-08696.1999
32. Maren, S., Aharonov, G., & Fanselow, M. S. (1996). Retrograde abolition of conditional fear after excitotoxic lesions in the basolateral amygdala of rats: Absence of a temporal gradient. *Behavioral Neuroscience*, *110*(4), 718–726. https://doi.org/10.1037/0735-7044.110.4.718
33. Martin-Fernandez, M., Jamison, S., Robin, L. M., Zhao, Z., Martin, E. D., Aguilar, J., Benneyworth, M. A., Marsicano, G., & Araque, A. (2017). Synapse-specific astrocyte gating of amygdala-related behavior. *Nature Neuroscience*, *20*(11), 1540. https://doi.org/10.1038/NN.4649
34. Parpura, V., Basarsky, T. A., Liu, F., Jeftinija, K., Jeftinija, S., & Haydon, P. G. (1994). Glutamate-mediated astrocyte-neuron signaling. *Nature*, *369*(6483), 744–747. https://doi.org/10.1038/369744A0
35. Perea, G., & Araque, A. (2005). Glial calcium signaling and neuron–glia communication. *Cell Calcium*, *38*(3–4), 375–382. https://doi.org/10.1016/J.CECA.2005.06.015
36. Perea, G., Navarrete, M., & Araque, A. (2009). Tripartite synapses: astrocytes process and control synaptic information. *Trends in Neurosciences*, *32*(8), 421–431. https://doi.org/10.1016/J.TINS.2009.05.001
37. Porter, J. T., & McCarthy, K. D. (1997). ASTROCYTIC NEUROTRANSMITTER RECEPTORS IN SITU AND IN VIVO. *Progress in Neurobiology*, *51*(4), 439–455. https://doi.org/10.1016/S0301-0082(96)00068-8
38. Qin, H., He, W., Yang, C., Li, J., Jian, T., Liang, S., Chen, T., Feng, H., Chen, X., Liao, X., & Zhang, K. (2020). Monitoring Astrocytic Ca2+ Activity in Freely Behaving Mice. *Frontiers in Cellular Neuroscience*, *14*, 410. https://doi.org/10.3389/FNCEL.2020.603095/XML/NLM

39. Sengupta, A., Yau, J. O. Y., Jean-Richard-dit-Bressel, P., Liu, Y., Millan, E. Z., Power, J. M., & McNally, G. P. (2018). Basolateral Amygdala Neurons Maintain Aversive Emotional Salience. *The Journal of Neuroscience*, *38*(12), 3001. https://doi.org/10.1523/JNEUROSCI.2460-17.2017
40. Shelkar, G. P., Liu, J., & Dravid, S. M. (2021). Astrocytic NMDA Receptors in the Basolateral Amygdala Contribute to Facilitation of Fear Extinction. *International Journal of Neuropsychopharmacology*, *24*(11), 907–919. https://doi.org/10.1093/IJNP/PYAB055
41. Stehberg, J., Moraga-Amaro, R., Salazar, C., Becerra, A., Echeverría, C., Orellana, J. A., Bultynck, G., Ponsaerts, R., Leybaert, L., Simon, F., Sáez, J. C., & Retamal, M. A. (2012). Release of gliotransmitters through astroglial connexin 43 hemichannels is necessary for fear memory consolidation in the basolateral amygdala. *The FASEB Journal*, *26*(9), 3649–3657. https://doi.org/10.1096/FJ.11-198416
42. Steinman, M. Q., Gao, V., & Alberini, C. M. (2016). The role of lactate-mediated metabolic coupling between astrocytes and neurons in long-term memory formation. *Frontiers in Integrative Neuroscience*, *10*(MAR2016), 10. https://doi.org/10.3389/FNINT.2016.00010/XML/NLM
43. Tsunematsu, T., Sakata, S., Sanagi, T., Tanaka, K. F., & Matsui, K. (2021). Region-Specific and State-Dependent Astrocyte Ca2+ Dynamics during the Sleep-Wake Cycle in Mice. *Journal of Neuroscience*, *41*(25), 5440–5452. https://doi.org/10.1523/JNEUROSCI.2912-20.2021
44. Van Den Herrewegen, Y., Sanderson, T. M., Sahu, S., de Bundel, D., Bortolotto, Z. A., & Smolders, I. (2021). Side-by-side comparison of the effects of Gq- and Gi-DREADD-mediated astrocyte modulation on intracellular calcium dynamics and synaptic plasticity in the hippocampal CA1. Molecular Brain, 14(1), 1–13. https://doi.org/10.1186/S13041-021-00856-W/TABLES/1
45. Volterra, A., & Meldolesi, J. (2005). Astrocytes, from brain glue to communication elements: the revolution continues. *Nature Reviews Neuroscience 2005 6:8*, *6*(8), 626–640. https://doi.org/10.1038/nrn1722
46. Zhang, X., & Li, B. (2018). Population coding of valence in the basolateral amygdala. *Nature Communications 2018 9:1*, *9*(1), 1–14. https://doi.org/10.1038/s41467-018-07679-9
47. Zheng, J., Anderson, K. L., Leal, S. L., Shestyuk, A., Gulsen, G., Mnatsakanyan, L., Vadera, S., Hsu, F. P. K., Yassa, M. A., Knight, R. T., & Lin, J. J. (2017). Amygdala-hippocampal dynamics during salient information processing. *Nature Communications 2017 8:1*, *8*(1), 1–11. https://doi.org/10.1038/ncomms14413

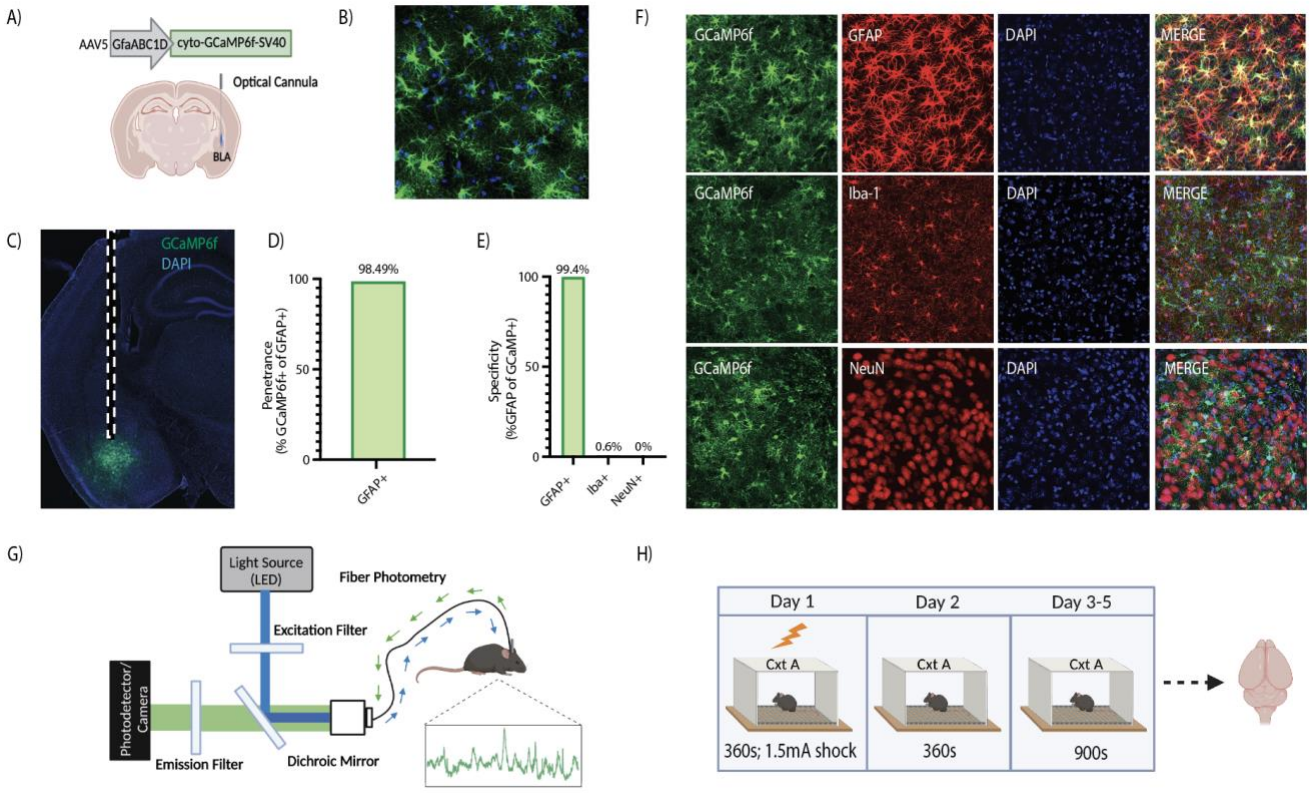

Figure 1. Population-level calcium recordings of basolateral amygdala astrocytes across contextual fear conditioning, recall and extinction. (A) Viral strategy and fiber implantation strategy for shock and no shock conditions. The genetically-encoded calcium indicator (GECI) AAV5-GfaABC1D-cyto-GCaMP6f-SV40 was unilaterally injected into the BLA region of wild type mice. (B) Representative image of GFAP-GCaMP6f+ (green) and DAPI+ (blue) cell expression within the BLA at 20x magnification and (C) 10x magnification. Dashed white lines indicate the approximate location of the unilateral fiber implantation. (D) Penetrance of GCaMP6f (2251 GCaMP6f+/2381 GFAP+ = 98.49%) (n=3; 4 slices/mouse). (E) Specificity of GCaMP6f (4 Iba-1+/662 GCaMP6f+ = 0.604% microglia; 0 NeuN+/1064 GCaMP6f+ = 0.00% neurons; 2242 GFAP+/2256 GCaMP6f+ = 99.4% astrocyte)(n=3; 4 slices/mouse). (F) Representative expression of GCaMP6f expression, and overlap with microglial (Iba-1), astrocytic (GFAP) and neuronal (NeuN) markers. (G) *In vivo* fiber photometry set-up; a 470-nm LED delivered an excitation wavelength to GCaMP6f-expressing astrocytes via a patch cord and single fiber optic implant in freely moving mice. The emitted 530-nm signal from the indicator was collected via the same patch cord and fiber, spectrally-separated using a dichroic mirror, passed through a series of filters and focused on a scientific camera. A representative calcium time series trace is shown for astrocytic calcium. Calcium-independent isosbestic signal was recorded simultaneously to account for motion, tissue autofluorescence and photobleaching across time. (H) Behavioral paradigm; mice underwent contextual fear conditioning (CFC) on Day 1 in Context A (Cxt A) for 360 seconds where they received 4, 1.5mA foot shocks. Day 2, mice were placed back into Cxt A for contextual recall for 360 seconds in the

absence of foot shock. Days 3-5, mice underwent three contextual extinction sessions for 900 seconds each. Mice were perfused and brains extracted for histological assessment.

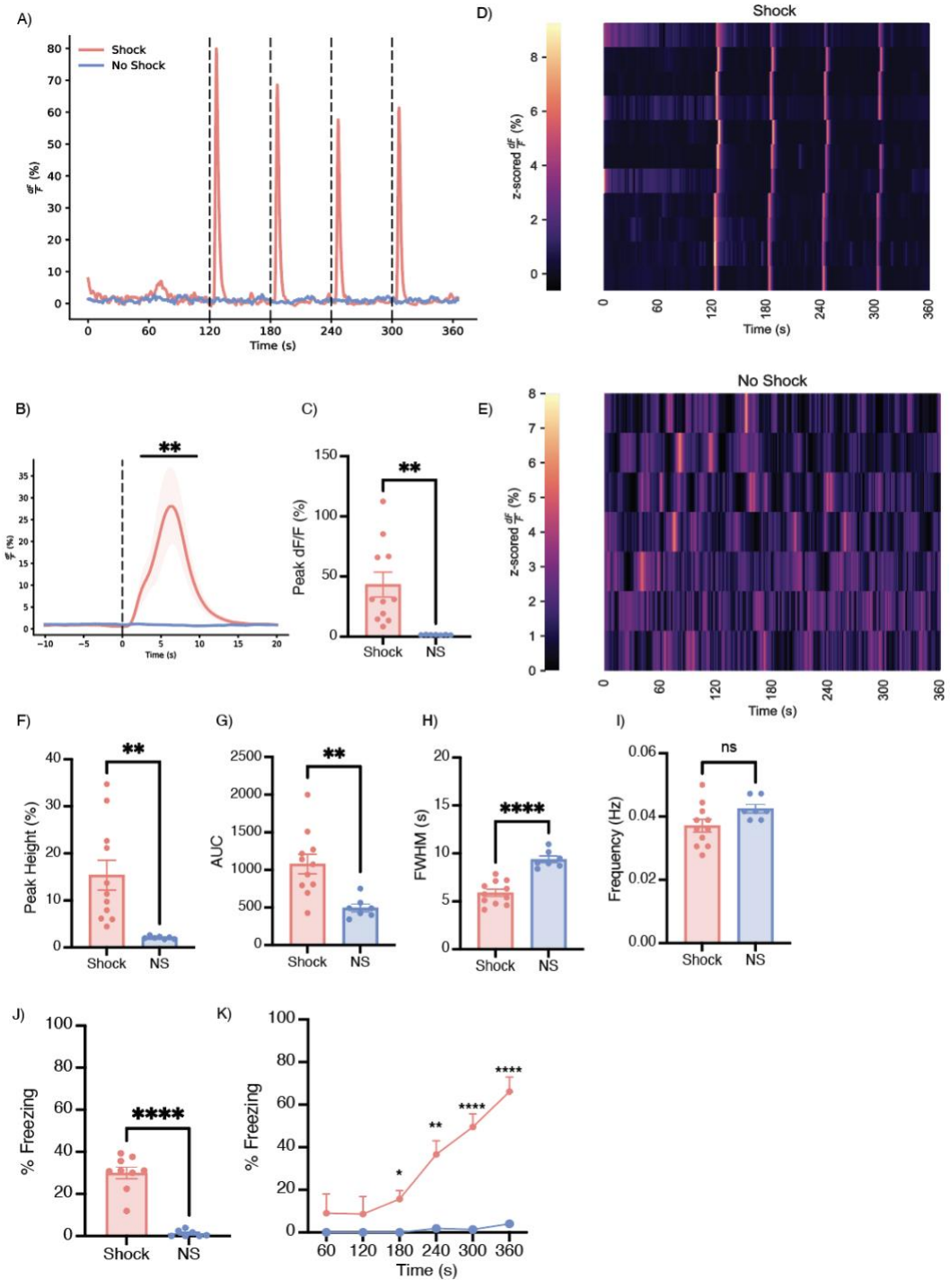

Figure 2. Basolateral amygdala astrocytes robustly respond to foot shock during contextual fear conditioning and exhibit unique calcium event dynamics compared to no-shock controls. (A) Representative calcium time series (dF/F %) for shock and no-shock conditions during the 360 second CFC session. 1.5mA foot shocks occurred at the 120, 180, 240 and 300 second time points, as indicated by vertical dashed lines. (B) Peri-event analysis for 1.5 mA foot shock, with the onset of foot shock occurring at the dashed line (time = 0). (C) Quantification of the average percent change in peak dF/F at the onset of foot shock. (D-E) Z-scored dF/F (%) across CFC for (D) shock and (E) no-shock conditions; each row represents a single subject across time within the session. (F-I) Calcium event metrics; (F) peak height, (G) area under the curve, (H) full-width half maximum, and (I) frequency. (J-K) Behavioral analysis; (J) average percent freezing and (K) freezing across time within the CFC session. Error bars indicate SEM. For t-tests and ANOVAs, $p \leq 0.05$, $^{**}p \leq 0.01$, $^{***}p \leq 0.001$, $^{****}p \leq 0.0001$, ns = not significant. For peri-event metrics, * = 95% CI; ** = 99% CI; *** =99.9, ns = not significant. Shock n=11, no-shock n=7.

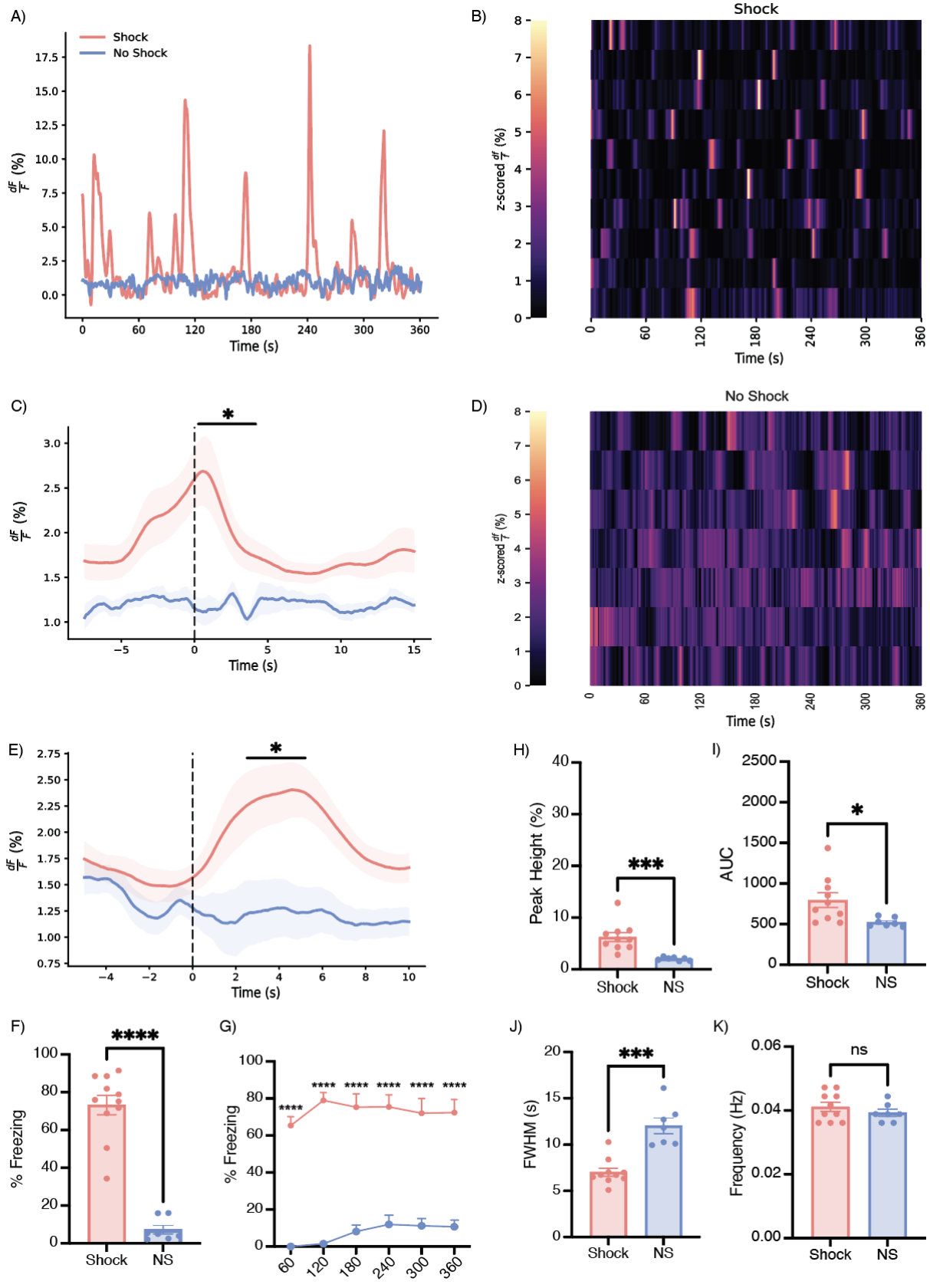

Figure 3. BLA astrocytes respond reliably to the onset and offset of freezing behavior during contextual recall. (A) Representative calcium time series (dF/F %) for shock and no-shock conditions during the 360 second recall session in the absence of foot shock. (B, D) Z-scored dF/F (%) across recall for (B) shock and (D) no-shock conditions; each row represents a single subject across time within the session. (C, E) Peri-event analysis for the onset (C) and offset (E) of freezing behavior, with each event occurring at the dashed line (time = 0). (F-G) Behavioral analysis; (F) average percent freezing and (G) freezing across time within the recall session. (H-K) Calcium event metrics; (H) peak height, (I) area under the curve, (J) full-width half maximum, and (K) frequency. Error bars indicate SEM. For t-tests and ANOVAs, $p \leq 0.05$, $^{**}p \leq 0.01$, $^{***}p \leq 0.001$, $^{****}p \leq 0.0001$, ns = not significant. For peri-event metrics, * = 95% CI; ** = 99% CI; *** = 99.9, ns = not significant. Shock n=11, no-shock n=7.

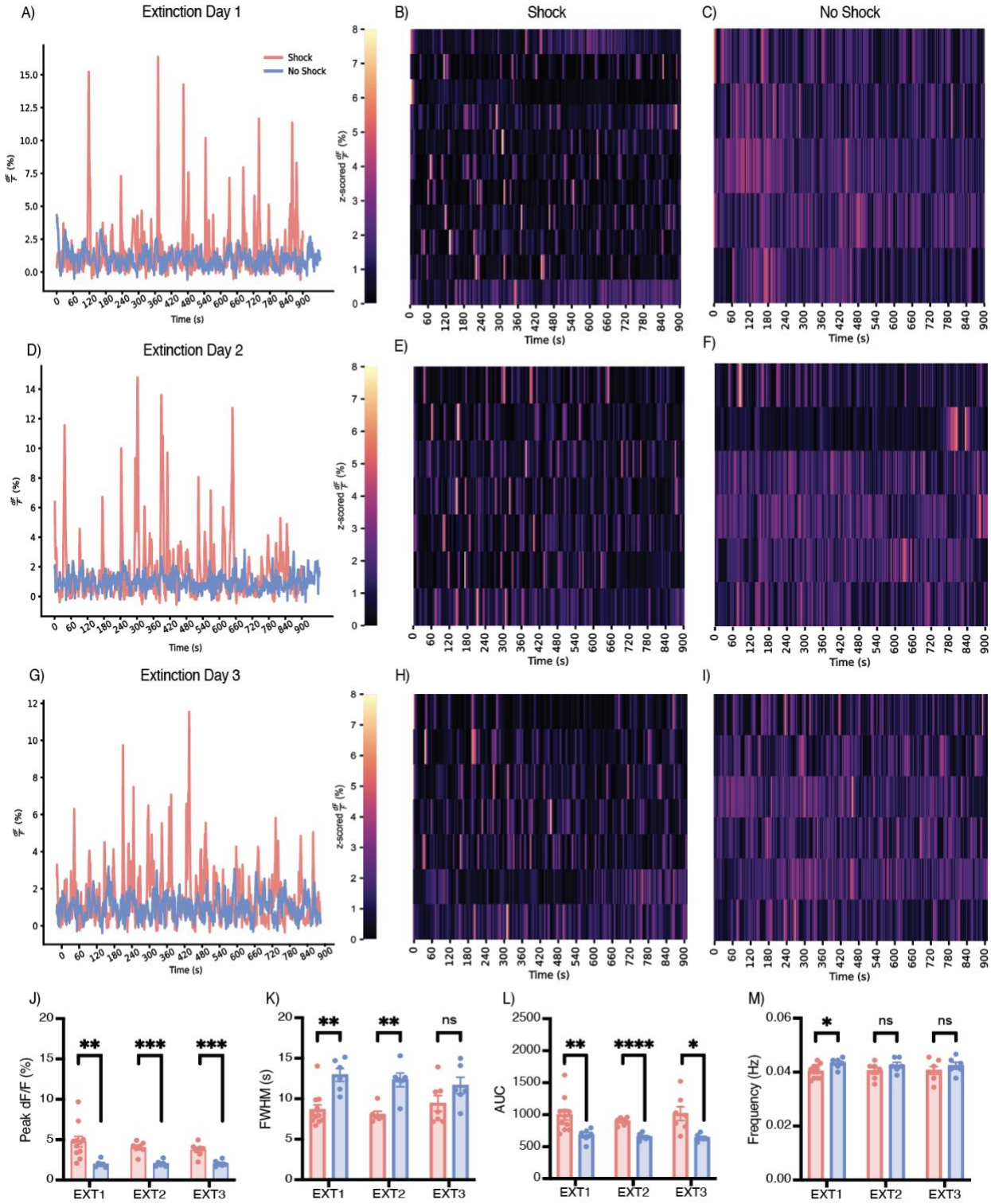

Figure 4. BLA astrocytes in the shock condition exhibit increased peak height, decreased duration, and increased total fluorescence of events compared to no-shock, but these do not change across extinction days. (A, D, G) Representative calcium time series (dF/F %) for shock and no-shock conditions during the 900 second contextual extinction sessions; (A) extinction day 1, (D) extinction day 2, (G) extinction day 3. (B, E, H) Z-scored dF/F (%) across extinction for shock condition; each row represents a single subject across time within the session. (C, F, I) Z-scored dF/F (%) across extinction for the no-shock condition; each row represents a single subject across time within the session. (J-M) Calcium event metrics; (J) peak height, (K) full-width half maximum, (L) area under the curve, and (M) frequency across all three days of extinction. Error bars indicate SEM. For t-tests, $p \leq 0.05$, $^{**}p \leq 0.01$, $^{***}p \leq 0.001$, $^{****}p \leq 0.0001$, ns = not significant. Extinction 1: shok n=11, no-shock=6 (For the no-shock group, one animal's recording was approx 90 seconds, short. This animal was excluded from the raster plot and behavioral analysis, but still used for event metric calculations). Extinction 2: shock n=7, no-shock=6. Extinction 3 : shock n=7, no-shock=6.

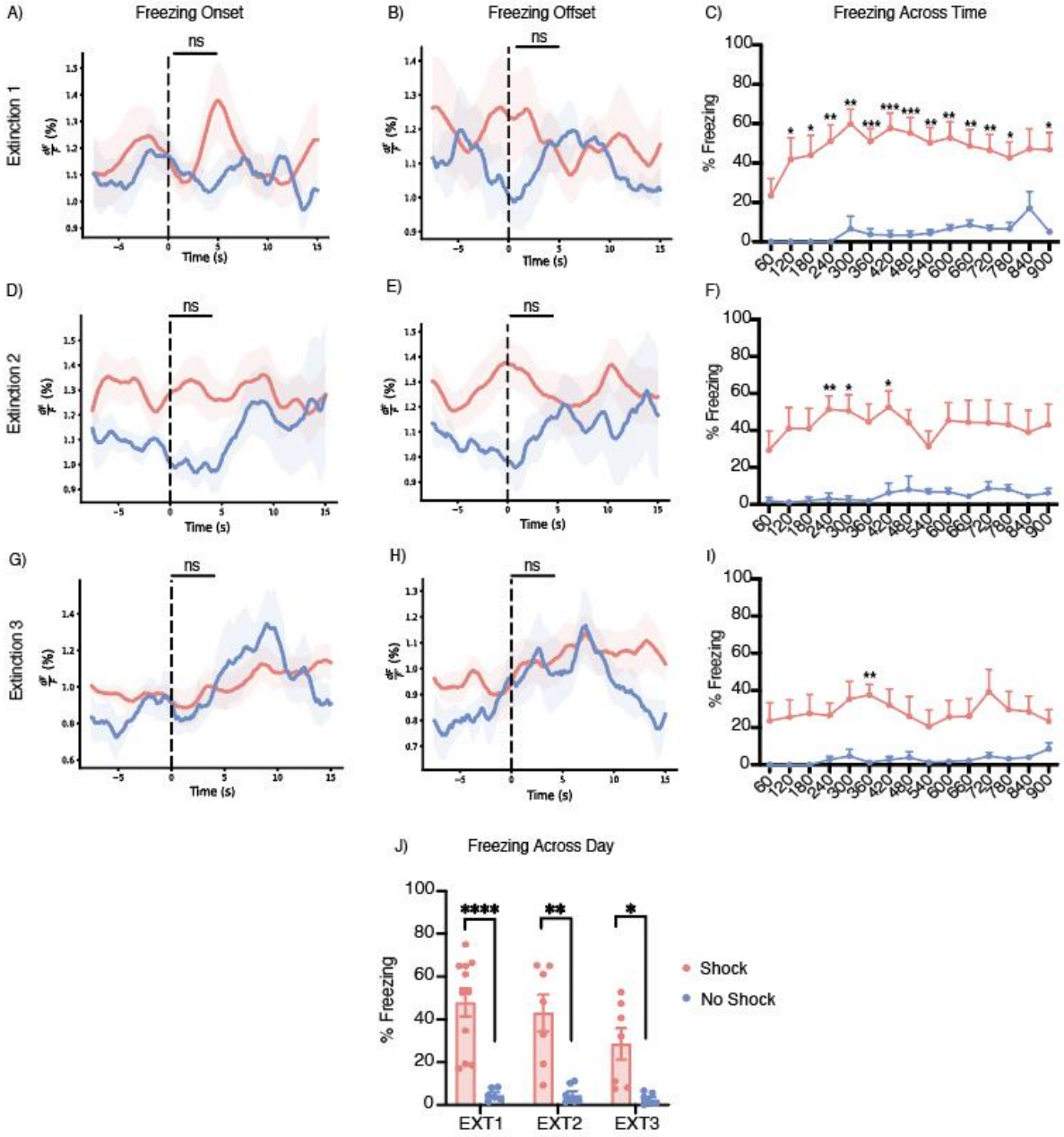

Figure 5. BLA astrocytic calcium does not respond to the onset or offset of freezing behavior during extinction sessions. (A-B) Peri-event analysis for the onset (A) and offset (B) of freezing behavior, with each event occurring at the dashed line (time = 0) for extinction day 1. (D-E) Peri-event analysis for the onset (D) and offset (E) of freezing behavior, with each event occurring at the dashed line (time = 0) for extinction day 2. (G-H) Peri-event analysis for the onset (G) and offset (H) of freezing behavior, with each event occurring at the dashed line (time = 0) for extinction day 3. (C, F, I) Percent freezing across time within (C) extinction day 1, (F) extinction day 2 and (I) extinction day 3. (J) Average percent freezing across three days of extinction for shock and no-shock conditions. Error bars indicate SEM. For t-tests and ANOVAs,

p ≤ 0.05, **p ≤ 0.01, ***p ≤ 0.001, ****p ≤ 0.0001, ns = not significant. For peri-event metrics, * = 95% CI; ** = 99% CI; *** = 99.9, ns = not significant. Extinction 1: shock n=11, no-shock=6 (For the no-shock group, one animal's recording was approx 90 seconds, short. This animal was excluded from the raster plot and behavioral analysis, but still used for event metric calculations). Extinction 2: shock n=7, no-shock=6. Extinction 3: shock n=7, no-shock=6.